



# Interaction of Bioactive Compounds of *Moringa oleifera* Leaves with SARS-CoV-2 Proteins to Combat COVID-19 Pathogenesis: a Phytochemical and In Silico Analysis

Sahabjada Siddiqui<sup>1</sup> · Shivbrat Upadhyay<sup>1</sup> · Rumana Ahmad<sup>2</sup> · Md. Abul Barkat<sup>3</sup> · Azfar Jamal<sup>4,5</sup> · Abdulaziz S. Alothaim<sup>5</sup> · Mohd. Zaheen Hassan<sup>6</sup> · Mohammad Akhlaquer Rahman<sup>7</sup> · Md Arshad<sup>8</sup> · Tanveer Ahamad<sup>1</sup> · Mohammad Faheem Khan<sup>1</sup> · Hari Shankar<sup>9</sup> · M. Ali<sup>10</sup> · Sarjeel Kaleem<sup>11</sup> · Jalal Ahmad<sup>12</sup>

Accepted: 24 June 2022 / Published online: 15 July 2022

© The Author(s), under exclusive licence to Springer Science+Business Media, LLC, part of Springer Nature 2022

## Abstract

Novel SARS-CoV-2 claimed a large number of human lives. The main proteins for viral entry into host cells are SARS-CoV-2 spike glycoprotein (PDB ID: 6VYB) and spike receptor-binding domain bound with ACE2 (spike RBD-ACE2; PDB ID: 6M0J). Currently, specific therapies are lacking globally. This study was designed to investigate the bioactive components from *Moringa oleifera* leaf (MOL) extract by gas chromatography-mass spectroscopy (GC-MS) and their binding interactions with spike glycoprotein and spike RBD-ACE2 protein through computational analysis. GC-MS-based analysis unveiled the presence of thirty-seven bioactive components in MOL extract, viz. polyphenols, fatty acids, terpenes/triterpenes, phytosterols/steroids, and aliphatic hydrocarbons. These bioactive phytoconstituents showed potential binding with SARS-CoV-2 spike glycoprotein and spike RBD-ACE2 protein through the AutoDock 4.2 tool. Further by using AutoDock 4.2 and AutoDock Vina, the top sixteen hits (binding energy  $\geq -6.0$  kcal/mol) were selected, and these might be considered as active biomolecules. Moreover, molecular dynamics simulation was determined by the Desmond module. Interestingly two biomolecules, namely  $\beta$ -tocopherol with spike glycoprotein and  $\beta$ -sitosterol with spike RBD-ACE2, displayed the best interacting complexes and low deviations during 100-ns simulation, implying their strong stability and compactness. Remarkably, both  $\beta$ -tocopherol and  $\beta$ -sitosterol also showed the drug- likeness with no predicted toxicity. In conclusion, these findings suggested that both compounds  $\beta$ -tocopherol and  $\beta$ -sitosterol may be developed as anti-SARS-CoV-2 drugs. The current findings of in silico approach need to be optimized using in vitro and clinical studies to prove the effectiveness of phytomolecules against SARS-CoV-2.

**Keywords** *Moringa oleifera* leaf · Phytoconstituents · GC-MS analysis · SARS-CoV-2 · Molecular docking

✉ Sahabjada Siddiqui  
sahabjadabiotech04@gmail.com

Extended author information available on the last page of the article

## Introduction

Coronaviruses are deadly infections that harm humans and animals alike. Among coronaviruses, severe acute respiratory syndrome coronavirus-2 (SARS-CoV-2) was detected as a novel coronavirus in China in December 2019, which results in an outbreak in numerous countries. Later in March 2020, coronavirus-induced infectious respiratory disease was called coronavirus disease (COVID-19), and it was declared a pandemic by the World Health Organization [1]. Since this pandemic is affecting millions of people across the globe, various preventive measurements like application of disinfectants, sanitizers, social distancing, mandatory wearing of masks, and quarantine of suspected or infected individuals are being used to counter the COVID-19 infection [2]. However, despite prophylactic and curative efforts, the number of COVID-19-positive cases is at rising since its outbreak. Therefore, the current preventive and therapeutic approaches have proven to be insufficient to combat the SARS-CoV-2. As a result, finding alternative therapies to prevent the spread of this lethal virus is critical.

SARS-CoV-2 belongs to the *Coronaviridae* family, and its genetic material is single-stranded-positive-sense RNA, approximately 26–32 kb in size [3, 4]. The key structural proteins of SARS-CoV-2 are spike glycoprotein, nucleocapsid protein, and envelope protein. The spike glycoproteins of SARS-CoV-2 are the primary targets of drugs because they aid SARS-CoV-2 entry into host cells by binding to the angiotensin-converting enzyme 2 (ACE2) receptor in humans [5, 6]. Therefore, SARS-CoV-2 spike glycoprotein (PDB ID: 6VYB) and spike receptor-binding domain bound with ACE2 (spike RBD-ACE2; PDB ID: 6M0J) were selected as target protein in the present study.

Natural resources are rich source of active components that can be used to develop novel drugs. Numerous herbal plants are found in the Indian subcontinent that is employed in traditional medicine [7]. Ayurveda plants can provide biologically active components with greater activity and/or lower toxicity [8]. The plant *Moringa oleifera* Lam. belongs to the Moringaceae family and is commonly cultivated in the tropics. The *Moringa oleifera* plant is native to the Himalayan foothills in northwestern India and is extensively distributed in Pacific Islands, Asia, and Africa. Horseradish tree and drumstick tree are two common names for it and often known to as “tropical natural nutrition.” The plant’s leaves, seeds, fruit pods, and roots all contain essential nutritional supplements as well as therapeutic characteristics [10]. Various pharmacological properties comprising antioxidant, anti-inflammatory, anti-microbial, anti-fibrotic, anti-hyperglycemic, and anti-tumor activities have been credited to several components of this multipurpose tree [11, 12]. Because of its high nutraceutical value, *Moringa oleifera* leaves possess extremely important therapeutic and medicinal properties [13]. *Moringa oleifera*’s high and unique immunological perspective leads to a hypothesis to examine the antiviral efficacy against COVID-19 illness.

*Moringa oleifera*, Lam. leaves were taken for phytochemical analysis using the gas chromatography-mass spectroscopy (GC-MS) technique. Approximately thirty-seven phytochemicals from the phytosterols, polyphenols, terpenes, fatty acids, and aliphatic hydrocarbon classes were identified. To explore possible hits against SARS-CoV-2, these phytochemicals were evaluated using in silico molecular docking, toxicity potential, and drug-likeness prediction. The top sixteen hits of *Moringa oleifera*’s components displayed a high affinity for the SARS-CoV-2 spike glycoprotein and spike RBD-ACE2 protein. Further, the best binding interacting complexes, viz.  $\beta$ -tocopherol-spike glycoprotein and  $\beta$ -sitosterol-spike RBD-ACE2 complexes, displayed strong stability and compactness during the 100-ns simulation. The top sixteen phytoconstituents including  $\beta$ -tocopherol

and  $\beta$ -sitosterol displayed drug- likeness with no expected toxicity which needs to be optimized using in vitro and clinical studies for drug development.

## Materials and Methods

### Extract Preparation from Plant Materials

The fresh plant (ID No. IU/PHAR/HRB/14/07) was collected from Lucknow City, India, and identified by the Pharmacognosy Department at the Integral University, Lucknow. Soxhlet apparatus was used to prepare 95% ethanolic extract of MOL. The extracted materials were stored at 4 °C for further GC–MS study.

### GC–MS Examination

GC–MS is a preferable technology for the chemical characterization of herbal extract. The phyto-composition of MOL extract was assessed by GC–MS-QP2010 Plus system (Shimadzu, Japan) with an RTX-5 MS (Restek) from the Advanced Instrumentation Facility, JNU, New Delhi. Approximately 1  $\mu$ l of diluted MOL extract was injected at a split ratio 10:0 onto an RTX-5 column (internal diameter, 60 m $\times$ 0.25 mm and film thickness, 0.25  $\mu$ m). At 90.4-kPa inlet pressure, a continuous flow rate of 1.21 ml/min of helium gas was used as a carrier. The remaining programs were set as per the previously published procedure [14]. A mass spectrophotometer was used to separate the plant extract into numerous constituents with varied retention periods for chemical identification. A chromatogram of intensity against retention time was created using software connected to the mass spectrophotometer. NIST08s.LIB and WILEY8.LIB chemical libraries were employed to detect the mass spectra of unknown constituents with spectra of known constituents and ascertained their name, structure, molecular weight, and m/z values.

### In Silico Prediction and Computational Analysis

#### Ligand Preparation

The identified phytochemicals of MOL were selected for ligand preparation. The 3-D structures were downloaded from the PubChem website [15], and energy minimization was executed by Merck Molecular Force Field (MMFF94). The structures of all ligands were optimized using AutoDock Tools (ADT) version 4.2.

#### Protein Preparation

The 3-D crystal structures of SARS-CoV-2 spike glycoprotein (PDB ID: 6VYB) and spike receptor-binding domain bound with ACE2 (spike RBD-ACE2; PDB ID: 6M0J) were obtained from the Protein Data Bank. For molecular docking studies, complete PDB structures of proteins were chosen. All 3D protein structures were refined as per previously published work [15]. AccelrysBiovia Discovery Studio version 2017 R2 (Biovia, USA) was applied for the visualization of docked complex molecules.

## AutoDock 4.2 and AutoDock Vina

Molecular docking of phytoconstituents was performed on two selected protein targets of SARS-CoV-2 through AutoDock 4.2 and AutoDock Vina [16]. Autogrid was utilized to calculate the positioning of the ligand on binding site of the protein using a grid spacing of 0.375 and grid coordinates (X, Y, and Z) axes of  $60 \times 60 \times 60$ . Ten runs of Lamarckian genetic algorithm (GA) were performed, and the output binding energies (B.E.) and dissociation constant ( $K_d$ ) values were analyzed [14]. The best docking results obtained were validated using further docking software AutoDock Vina. The best docking orientations (lowest binding energy and  $K_d$  value) were analyzed using Discovery Studio and PyMOL molecular graphic system.

## Analysis of Molecular Dynamics (MD) Simulation

Desmond module (Schrodinger Release 2020–4) package was employed for MD simulation analysis of best-binding interacting complexes, viz.  $\beta$ -tocopherol complexed with spike glycoprotein (PDB ID: 6VYB) and  $\beta$ -sitosterol in complex with spike receptor binding domain binding to ACE2 (spike RBD-ACE2; PDB ID: 6M0J). All the simulations were performed in triplicates for more concrete data analysis. The TIP3P water model was explored for system solvation, and water-soaked-solvated system was formed in Desmond module of the System Builder tool. A buffer distance of around 10 Å from the protein's outer surface was used to construct the orthorhombic box with periodic boundary conditions. OPLS-3e force field was employed to run MD simulation. An adequate quantity of counterions was supplemented to neutralize the system. Following the addition of 0.15 M NaCl to the simulation box, the iso-osmotic state was maintained. A defined equilibration procedure was applied before the simulation's production run. After equilibration, the unrestrained production phase was conducted for 100 ns under NPT ensemble at 300 K temperature and 1.01 bar pressure. A total of 100 ns of simulation time was used, with 1000 frames stored to the trajectory. MD simulation trajectory was analyzed through simulation interaction diagram using RMSD, RMSF, radius of gyration (Rg), hydrogen bond analysis, and histogram for torsional bonds.

## PASS (Prediction of Activity Spectra for Substances) Program: Lipinski's Rule of Five

Based on the structure–activity association, PASS predicts biological and pharmacological properties, as well as probable side effects and mode of action of compounds [17]. Lipinski's rule of five was employed to calculate the drug-likeness of phytoconstituents using the online application of Molinspiration.

## Toxicity Potential Study

Toxicity risk assessment offers preliminary information of possible side effects of phytoconstituents for prediction of new drug development at a nearly stage. OSIRIS Data

Warrior V5.2.1 software was used to observe drug- likeness and drug-toxicity risk characteristics such as tumorigenic, mutagenic, reproductive, and irritating effects [18].

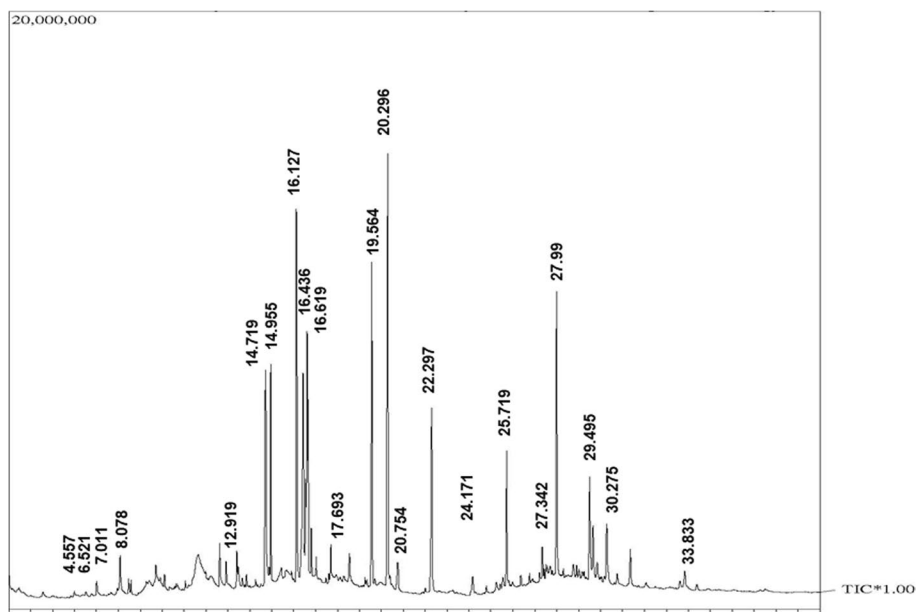
## Physicochemical and Pharmacokinetic Property Prediction

The ADMET properties of identified components were predicted through the online SwissADME software. This software analyzes important physicochemical properties, pharmacokinetic properties, and medicinal chemistry friendliness of compounds such as distribution (skin permeability and blood–brain barrier), its metabolism (P-glycoprotein substrate and cytochrome P450) and lipophilicity for plasma membrane absorption [19].

## Results and Discussion

### GC–MS Analysis of *Moringa oleifera* Leaf

Chemotyping of herbal extract is critical for therapeutically validation and determination of the traditionally used plant parts. As revealed by a previous study, mass spectra of particular metabolites are useful in identifying such metabolites present in total extract [20]. The nature and structure of the chemicals eluted at retention time are determined by the mass spectrometer [21]. As illustrated in Fig. 1, the GC–MS chromatogram of the native MOL alcoholic extract revealed approximately thirty-seven peaks indicating thirty-seven bioactive compounds of polyphenols, fatty acids, terpenes/triterpenes, phytosterols/steroids, and aliphatic hydrocarbons. The identified components from native MOL alcoholic extract, their retention time, molecular weight, and percent peak area



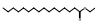
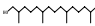
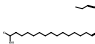
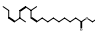
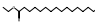


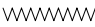
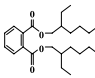

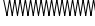

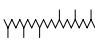
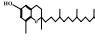
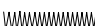
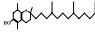
**Fig. 1** GC–MS total ion chromatogram (TIC) of the 95% ethanolic extract of *Moringa oleifera* leaf. Total ion current is represented by Y-axis and retention time by X-axis

**Table 1** Identification of phytoconstituents from 95% ethanolic *Moringa oleifera* leaf extract by GC–MS analysis

S. No.	Compounds Name	Structure	Canonical SMILES	Pub Chem CID	MF	MW	Area %	RT	Nature	Fragmentations (m/z)
1.	4H-Pyran-4-one, dihydro-3,5-dihydroxy-6-methyl-		CC1=C(C(=O)C(CO1)O)O	11983	C6H8	144.	0.1	4.5	Pyranone	43,101, 144
2.	4-morpholinepropanamine; N-(3-Aminopropyl)morpholine		C1COCCN1CCCN	61055	C7H16N2O	144.	0.1	6.5	Amine	100,56, 113
3.	Piperidine, (phenylmethyl)-[2-Benzylpiperidine]		C1CCNC(C1)CC2=CC=C C=C2	11800	C12H17N	175	0.4	7.0	Heterocyclic amine	84,56,3 9
4.	2-Furanmethanol, ethenyltetrahydro-alpha, alpha, 5-trimethyl-, trans- [Linalyl oxide]		CC1(CCC(O1)C(C)C(O)O)C=C	22310	C10H18O2	170.	0.9	8.0	Furan isomer	59,43,9 4
5.	N-[(E)-3-methylbutylidene]-2-phenylethanamine; Benzeneethanamine, N-(3-methylbutylidene)-		CC(C)CC=NCCC1=CC=C C=C1	53566	C13H19N	189.	0.2	8.5	Amine oxide	42,56,1 47
6.	Guanosine		C1=NC2=C(N1C3C(C(C(O3)CO)O)N=C(NC2=O)N		C10H13N5O5	283	0.5	9.4	Purine nucleoside	57,18,7 3
7.	Phenol, 2,4-bis(1,1-dimethylethyl)-; 2,4-Di-tert-butylphenol		CC(C)(C)C1=CC(=C(C=C(C=C1)O)C(C)(C)C	7311	C14H22O	206	0.5	9.7	Polyphenol	191,57, 206
8.	2(4h)-benzofuranone, 5,6,7,7a-tetrahydro-4,4,7a-trimethyl; Dihydroactinidiolide		CC1(CCCC2(C1=CC(=O)O2)C)C	27209	C11H16O2	180	0.2	10.	Terpene	111,43, 137
9.	Ethyl alpha-d-glucopyranoside; Ethyl hexopyranoside		CCOC1C(C(C(C(O1)O)O)O)O	91694	C8H16O5	208.	3.5	11.	glucopyranoside	60,42,7 3
10.	Tetradecanoic acid (Myristic acid)		CCCCCCCCCCCC(=O)O	11005	C14H28O2	228	1.1	12.	Fatty acid	60,73,4 1
11.	2(4h)-benzofuranone, 5,6,7,7a-tetrahydro-6-hydroxy-4,4,7a-trimethyl-, (6S-CIS)-; Loliolide		CC1(CC(C2C1=CC(=O)O2)C)O)C	10033	C11H16O3	196	0.6	12.	benzofuran	43,111, 178
12.	n-Hexadecanoic acid		CCCCCCCCCCCCCCCC(=O)O	985	C16H32O2	256	6.3	14.	Saturated	73,60,4

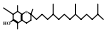
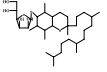
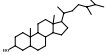
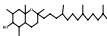
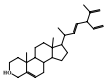
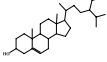
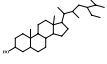
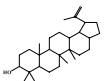
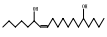
are listed in Table 1. The results revealed that the major constituents were found to be ethyl alpha-d-glucopyranoside (3.55%), n-hexadecanoic acid (6.39%), hexadecanoic acid, ethyl ester (3.43%), 2-hexadecen-1-ol, 3,7,11,15-tetramethyl, [R-[R\*,R\*-(E)]]- (8.14%), 9,12,15-Octadecatrienoic acid (Z,Z,Z)- (6.50%), 9,12,15-octadecatrienoic acid, ethyl ester (Z,Z,Z)- (8.86%), hexacosane (6.80%), Bis(2-ethylhexyl) phthalate (12.51%), hexatriacontane (6.16%), heneicosane (2.93%), alpha-tocopherol-beta-D-mannoside (7.04%), and stigmast-5-en-3-ol (3 beta)-(2.80%). The minor phytoconstituents were 1,2-cyclopentanediol, 1-(1-methylethyl)-, trans (0.26%), piperidine, 2-(phenylmethyl)- (0.45%), 2-furanmethanol, 5-ethenyltetrahydro-alpha, alpha, 5-trimethyl-, trans- (0.96%), N-[(E)-3-methylbutylidene]-2-phenylethanamine (0.23%), guanosine (0.59%), phenol, 2,4-bis(1,1-dimethylethyl)- (0.54%), 2(4 h)-benzofuranone, 5,6,7,7a-tetrahydro-4,4,7a-trimethyl (0.25%), myristic acid (1.19%), 2(4 h)-benzofuranone, 5,6,7,7a-tetrahydro-6-hydroxy-4,4,7a-trimethyl-,

**Table 1** (continued)

	Palmitic acid		(=O)O	3202	9	719	fatty acid	3	
13.	Hexadecanoic acid, ethyl ester;		CCCCCCCCCCCCCCCC (=O)OCC	12366 3602	C18H 3	284 955	3.4 3	14. Fatty acid, ester	88,101, 70
	Ethyl palmitate								
14.	2-hexadecen-1-ol, 3,7,11,15-tetramethyl-, [R-[R*,R*-(E)]]; Phytol		CC(C)CCCC(C)CCCC(C) CCCC(=CCO)C	53662 44	C20H 400	296 4	8.1 127	16. Phytol	68,82,4 3
15.	9,12,15-Octadecatrienoic acid, (Z,Z,Z)-; Linolenic acid		CCC=CCC=CCC=CCCC CCCC(=O)O	52809 34	C18H 3002	278 0	6.5 436	16. Fatty acid, Linolenic acid	79,67,9 3
16.	9,12,15-Octadecatrienoic acid, ethyl ester, (Z,Z,Z)-; Ethyl linolenate		CCC=CCC=CCC=CCCC CCCC(=O)OCC	53674 60	C20H 3402	306 6	8.8 619	16. Fatty acid	79,67,9 5
17.	Octadecanoic acid, ethyl ester; Ethyl stearate		CCCCCCCCCCCCCCCC CC(=O)OCC	8122 4002	C20H 4002	312 6	0.7 803	16. Fatty acid ester	88,101, 43
18.	Heneicosane		CCCCCCCCCCCCCCCC CCCCC	12403 44	C21H 44	296 7	0.5 693	17. aliphatic hydrocarbon	57,71,4 3
19.	Eicosane		CCCCCCCCCCCCCCCC CCCC	8222 42	C20H 42	282 2	0.8 548	18. aliphatic hydrocarbon	57,71,4 3
20.	Hexacosane		CCCCCCCCCCCCCCCC CCCCCCCCCCCC	12407 54	C26H 54	366 0	6.8 564	19. Alkane	57,71,4 3
21.	Bis(2-ethylhexyl) phthalate		CCCC(C)COC(=O)C1 =CC=CC=C1C(=O)OCC(C)CCCC	8343 3804	C24H 3804	390 51	12. 296	20. Diester of phthalic acid	149,167 ,279
22.	Tetatriacontane		CCCCCCCCCCCCCCCC CCCCCCCCCCCCCCCC CC	26519 70	C34H 70	478 2	1.0 754	20. Alkane	57,71,4 3
23.	Hexatriacontane		CCCCCCCCCCCCCCCC CCCCCCCCCCCCCCCC CCCC	12412 74	C36H 74	506 6	6.1 297	22. Alkane	57,71,4 3
24.	Docosanoic acid, ethyl ester; Ethyl docosanoate		CCCCCCCCCCCCCCCC CCCCCC(=O)OCC	22199 4802	C24H 4802	368 4	0.7 171	24. Fatty acid ester	88,43,5 7
25.	Squalene		CC(=CCCC(=CCCC(=CC CC=C(C)CCC=C(C)CCC =C(C)C)C)C	63807 2	C30H 50	410 9	0.1 795	24. Precursor of stigmasterol	69,81,9 5
26.	2,8-dimethyl-2-(4,8,12-trimethyltridecyl)-6-chromanol		CC1=CC(=CC2=C1OC(C C2)(C)CCCC(C)CCCC(C) CCCC(C)O	58653 7	C27H 4602	402 6	0.3 239	25. Delta-tocopherol, Vit. E	137,177 ,43
27.	Tetretetracontane		CCCCCCCCCCCCCCCC CCCCCCCCCCCCCCCC CCCCCCCCCCCC	23494 90	C44H 90	618 3	2.9 719	25. Alkane	57,71,4 3
28.	beta-Tocopherol		CC1=CC(=C(C2=C1OC( CC2)(C)CCCC(C)CCCC(	68574 47	C28H 4802	416 4	0.1 219	27. Tocopherol	416,151 ,43

(6S-CIS)- (0.61%), 2,6,10-trimethyl,14-ethylene-14-pentadecne (0.60%), octadecanoic acid, ethyl ester (0.76%), 2,6,10-trimethyl,14-ethylene-14-pentadecne (0.39%), tetretetracontane (0.57%), eicosane (0.82%), tetatriacontane (1.02%), docosanoic acid, ethyl ester (0.74%), 2,8-dimethyl-2-(4,8,12-trimethyltridecyl)-6-chromanol (0.36%), gamma-tocopherol (0.56%), ergost-5-en-3-ol, (3beta)- (0.43%), dl-alpha-Tocopherol (0.26%), stigmasta-5,22-dien-3-ol, (3beta,22e)- (0.24%), fucosterol (1.24%), lupeol (1.80%), 2,6,10-trimethyl,14-ethylene-14-pentadecne (1.01%), and E,E,Z-1,3,12-nonadecatriene-5,14-diol (0.56%). All other components were identified in trace amounts. A prior study has used GC-MS analysis to identify fifty-six bioactive compounds from a methanolic extract of *Tinospora crispa*, in which the top nine hits showed a strong affinity with the

**Table 1** (continued)

29.	gamma.-Tocopherol		C)CCCC(C)C)O CC1=C(C=C2CCC(OC2= C1C)(C)CCCC(C)CCCC( C)CCCC(C)C)O	92729 4802	C28H 48O2	416 6	0.5 342	27.	Tocopherol	151,416 ,191
30.	Alpha.-Tocopherol.-beta.- D-mannoside		CC1=C(C(=C(C2=C1OC( CC2)(C)CCCC(C)CCCC( C)CCCC(C)C)OC3C(C( C(O3)C(CO)O)O)O)C	59705 7 6007	C35H 6007	592 4	7.0 990	27.	Tocopherol	165,430 ,205
31.	Ergost-5-en-3-ol, (3.beta.)- ; Campesterol		CC(C)C(C)CCC(C)C1CC C2C1(CCC3C2CC=C4C3( CCC(C4)O)C)C	17318 3	C28H 480	400 3	0.4 757	28.	β-sitosterol	400,382 ,367
32.	dl.-alpha.-Tocopherol		CC1=C(C2=C(C(CCC(O2)( C)CCCC(C)CCCC(C)CC CC(C)C)C(=C1O)O)C	2116 5002	C29H 5002	430 6	0.2 900	28.	Vit. E	165,430 ,205
33.	Stigmasta-5,22-dien-3-ol, (3.beta.,22e)-		CCC(C=CC(C)C1CCC2C 1(CCC3C2CC=C4C3(CC C(C4)O)C)C)C(C)C	64327 45	C29H 480	412 4	0.2 010	29.	Steroids	55,83,4 12
34.	Stigmast-5-en-3-ol, (3.beta.)-; beta-Sitosterol		CCC(CCC(C)C1CCC2C1( CCC3C2CC=C4C3(CCC( C4)O)C)C)C(C)C	22228 4	C29H 500	414 0	2.8 495	29.	Steroids	396,381 ,414
35.	Fucoesterol		CC=C(CCC(C)C1CCC2C 1(CCC3C2CC=C4C3(CC C(C4)O)C)C)C(C)C	52813 28	C29H 480	412 4	1.2 650	29.	Steroids	314,55, 412
36.	Lupeol		CC(=C)C1CCC2(C1C3CC C4C5(CCC(C)C5CCC4(C 3(C2)C)C)C(C)O)C)C	25984 6	C30H 500	426 0	1.8 275	30.	Triterpene	43,68,4 26
37.	E,E,Z-1,3,12- Nonadecatriene-5,14-diol		CCCCC(C=CCCCCCC (C=CC=C)O)O	53647 68	C19H 3402	294 6	0.5 833	33.	Nonadeca- triene-diol	55,95,8 1

SARS-CoV-2 main protease (Mpro) enzyme [22]. Similarly, a recent study has found that *Ruellia prostrata* and *Senna tora* extracts contained a total of forty-three and fifty-three phytochemicals, respectively, identified through the GC–MS analytical method, in which the best four compounds were selected for future drug development based on molecular docking and MD simulation analyses [23]. The plant metabolites including terpenoids, polyphenols, and phytosterols of natural origin have potential pharmacological and medicinal applications in various stages of basic and clinical research. Previous reports have shown that plant metabolites such as polyphenols, phytosterols, and terpenoids have exerted antiviral activity against a wide range of viruses including HIV-1 and 2, HIV-2, HSV-1 and 2, adenovirus, Influenza A and B virus, dengue virus, RSV, CMV, infectious bronchitis virus (IBV), Ebola virus, Newcastle disease virus (NDV), poliomyelitis-1 virus, H1N1, lentivirus, and coronaviruses [24, 25]. Based on previous studies, the identified components in MOL extract were evaluated further for their virtual antiviral effects through molecular docking and MD simulation analysis which would contribute to the limited array of preventive and therapeutic medicines against COVID-19.

## Docking Analysis of MOL Phytoconstituents

Initially, AutoDock 4.2 was used to dock thirty-seven MOL phytochemicals towards SARS-CoV-2 spike glycoprotein and spike RBD-ACE2 protein. A total of seventy-four ( $37 \times 2 = 74$ ) binding combinations were generated, wherein top hits (binding energy  $\geq -6.0$  kcal/mol) were screened for further validation through AutoDock Vina

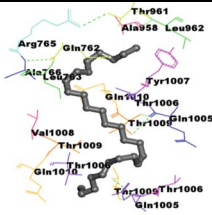
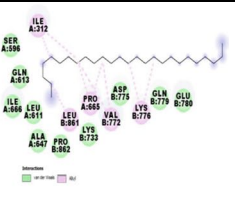
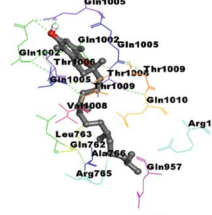
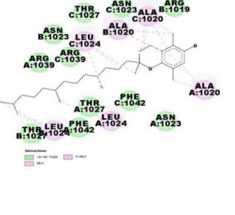

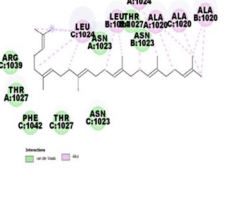
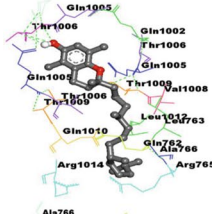
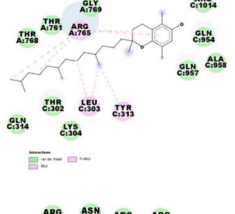
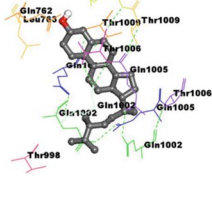
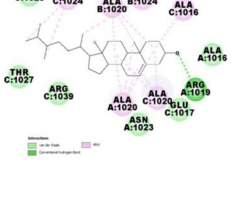


(Table S1). Tables 2 and 3 show the interacting amino acid residues in their binding pockets, dissociation constant ( $K_d$ ), and binding energy of spike glycoprotein and spike RBD-ACE2 protein with seven and thirteen phytoconstituents of MOL extract, respectively, through AutoDock 4.2 and AutoDock Vina tools.

Molecular docking analyses showed that E,E,Z-1,3,12- nonadecatriene-5,14-diol has the lowest docking effect ( $-6.13$  kcal/mol) and  $\beta$ -tocopherol exhibited the highest binding effect ( $-7.73$  kcal/mol) towards spike glycoprotein (Table 2). Binding interaction with spike RBD-ACE2 protein, compound  $\beta$ -tocopherol exhibited the lowest binding effect ( $-6.02$  kcal/mol), and  $\beta$ -sitosterol showed the highest binding effect ( $-8.66$  kcal/mol) (Table 3). While AutoDock Vina study showed tiny variations in the binding affinity of the sixteen bioactive components towards their receptors. These results suggested that minor differences in binding interaction of the phytoconstituents were due to variations in grid box generation and binding pockets determination on the target proteins through the docking tools (Tables 2 and 3). A previous study has shown the variations in the binding affinity of *Nigella sativa* phytoconstituents with NRBD of nucleocapsid protein and PLpro of SARS-CoV-2 with three different software AutoDock Vina, AutoDock 4.2, and iGEMDOCK 2.1 [16] support the findings of the current study. A previous study has reported the following active site residues of enzyme ACE2: Tyr515, Glu375, Pro346, His 345, His 505, and Arg 273 [26]. In this study, interacting amino acid residues of the active site are highlighted in gray color, as shown in Table 3. Based on molecular docking analyzes, several previous studies have revealed the many phytochemicals as spike glycoprotein and spike RBD-ACE2 protein inhibitors. For instance, as assessed by Maestro's Glide docking module, solanine, acetoside, rutin, and curcumin molecules exhibited docking scores of  $-9.50$ ,  $-8.52$ ,  $-7.91$ , and  $-7.15$  kcal/mol with SARS-CoV-2 spike RBD-ACE2 protein [27]. The amino acids Gln493, Lys417, Phe456, Tyr473, Tyr489, and Glu484 of Spike-RBD from SARS-CoV-2 have interacted prominently with the phytomolecule dicaffeoylquinic acid [28]. In a previously published study, the biomolecule floralginenoside B interacted with SARS-CoV-2 spike RBD (docking score =  $-8.61$  kcal/mol) with active pocket residues primarily through hydrogen bonds with Cys 480, Gln474, Glu465, Gly 482, and Asp467, while floralginsenoside E interacted with Glu471, Ser 459, Arg466, Asp467, and Arg 457 residues with binding score of  $-7.54$  kcal/mol [27]. In a recent investigation, phytochemicals from *Phyllanthus amarus* plant exhibited the strong binding affinity with spike glycoprotein of SARS-CoV-2 through AutoDock Vina, i.e., quercetin (BE =  $-8.8$  kcal/mol) interacting with amino acid residues Thr549, Asn978, Gly744, Arg1000, Thr573, Met740, and Tyr741; quercetin-3-O-glucoside (BE =  $-8.6$  kcal/mol) with Thr998, Arg995, and Asp994 residues; quercitrin (BE =  $-8.6$  kcal/mol) with Asp994 and Val991 residues; corilagin (BE =  $-9.5$  kcal/mol) with Thr998 and Agr995 residues; furosin (BE =  $-9.4$  kcal/mol) with Asp40, Arg567, Asp571, and Ser967 residues; and geraniin (BE =  $-10.1$  kcal/mol) with Glu988, Arg995, Tyr756, and Thr998 residues of spike glycoprotein [29].

In this study, based on their binding energies and  $K_d$  values,  $\beta$ -tocopherol and  $\beta$ -sitosterol were selected as the most effective antiviral components against SARS-CoV-2. Only cottonseed oil has considerable levels of  $\beta$ -tocopherol, which is found in low concentrations in many vegetable oils. It exhibits significant antioxidant activity, and its antiviral activity might be due to the presence of phenolic hydrogen on the 2H-1-benzopyran-6-ol nucleus [30]. The  $\beta$ -sitosterol is widely distributed in avocados, vegetable oil, nuts, and prepared foods such as salad dressings. The  $\beta$ -sitosterol has shown various pharmacological activities such as immunomodulatory, antibacterial activity, anti-inflammatory, and antioxidant activities [31, 32]. Also,  $\beta$ -sitosterol has shown potent antiviral

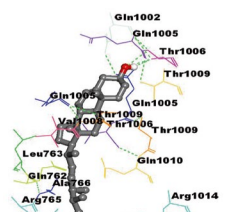
**Table 2** Docking effects of identified MOL phytoconstituents with spike glycoprotein (PDB ID: 6VYB) of SARS-CoV-2 through AutoDock 4.2 and AutoDockVina. AccelrysBiovia Discovery Studio version 2017 R2 was used to visualize interacting amino acid residues. In AutoDock 4.2, the ligand–protein interaction is represented by Ball and Stick model, while in AutoDockVina, it is represented by a 2-D line model. Dark green-dotted line represents the H-bond, and the alkyl and pi-alkyl bond interactions are represented by magenta broken lines

S. No.	Ligands with MF and MW and PubChem CID	AutoDock 4.2		AutoDock Vina		
		BE (Kcal/mol)	K <sub>d</sub> (μM)	BE (kcal/mol)	Interacting amino acids	
1.	Hexacosane PubChem CID: 12407 MF: C <sub>26</sub> H <sub>54</sub> MW: 366	-6.17	29.77 μM		-7.9	
2.	Hexatriacontane PubChem CID: 12412 MF: C <sub>36</sub> H <sub>74</sub> MW: 506	-6.42	19.74 μM		-8.1	
3.	Squalene PubChem CID: 638072 MF: C <sub>30</sub> H <sub>50</sub> MW: 410	-6.7	12.24 μM		-8.7	
4.	beta.-Tocopherol PubChem CID: 6857447 MF: C <sub>28</sub> H <sub>48</sub> O <sub>2</sub> MW: 416	-7.73	2.15 μM		-7.7	
5.	Ergost-5-en-3-ol, (3.beta.)- CAMPESTEROL PubChem CID: 173183 MF: C <sub>28</sub> H <sub>48</sub> O MW: 400	-6.33	22.74 μM		-8.6	

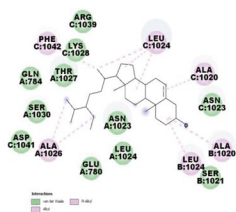
**Table 2** (continued)

6. Stigmast-5-en-3- $\alpha$ ,  
(3 $\beta$ .)-  
betaSitossterol

PubChem  
CID: 222284  
MF: C29H50O  
MW: 414

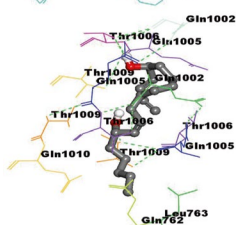


8.8

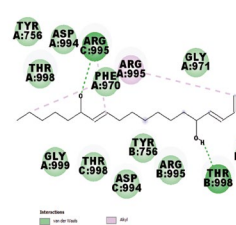


7. E,E,Z-1,3,12-  
Nonadecatriene-  
5,14-diol

PubChem  
CID: 5364768  
MF: C19H34O2  
MW: 294



-6.8



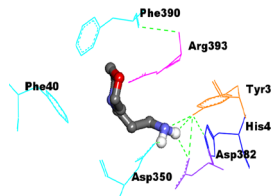
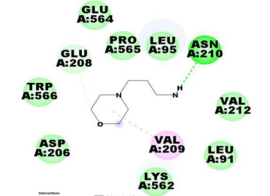
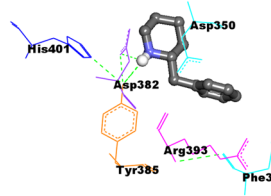
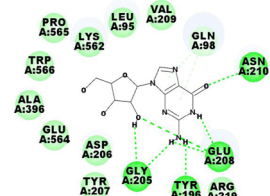
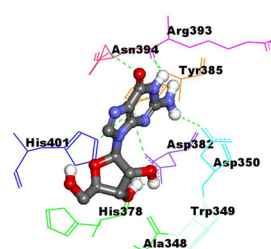
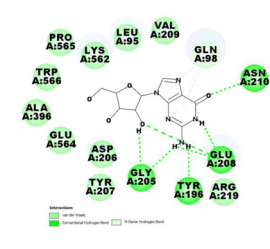
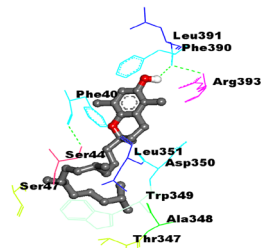
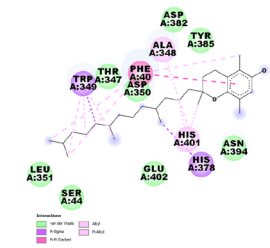
activity by protecting mice from lethal influenza A virus infection [33]. Interestingly, a recent study has supported our finding that  $\beta$ -sitosterol including other phytoconstituents has exhibited the highest affinity towards SARS-CoV-2 spike glycoprotein (closed state, PDB ID: 6VXX) and native human ACE2 receptor (PDB ID: 1R42) [34]. As structural protein spike glycoprotein of SARS-CoV-2 facilitates SARS-CoV-2 entry into host cells via angiotensin-converting enzyme 2 (ACE2) receptor in humans [5, 6], therefore, SARS-CoV-2 spike glycoprotein and spike receptor-binding domain bound with ACE2 could be used as therapeutic targets in the drug discovery process.

## Molecular Dynamics (MD) Simulation Analysis

RMSD measures the average variation in displacement of a group of atoms for a given frame compared to a reference frame, while RMSF is useful for characterizing local alterations along the protein chain [35, 36]. Monitoring the protein's RMSD provides the structural conformation throughout the simulation. Increasing or reducing the RMSD of a protein at the end of the simulation causes the system to become unequilibrated and pass a rigorous assessment.

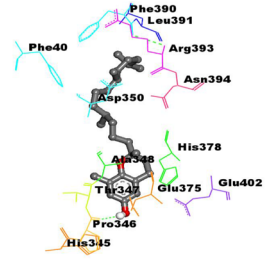
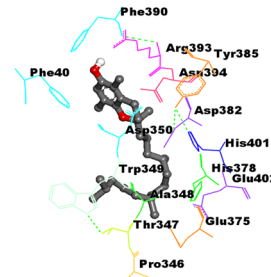
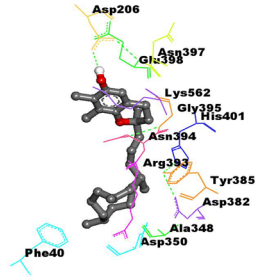
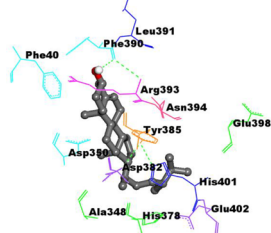
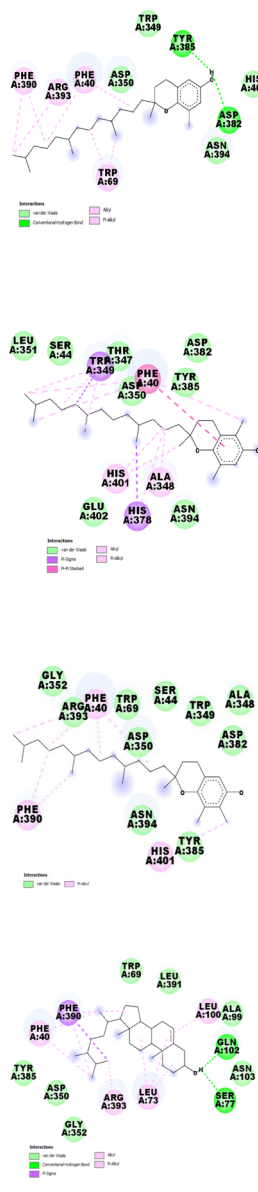
The stability of the docked complex of  $\beta$ -tocopherol with spike glycoprotein and  $\beta$ -sitosterol with spike RBD-ACE2 protein was investigated using Desmond module (Schrodinger Release 2020-2package) at a time scale of 100 ns in triplicate. From the obtained trajectory analysis of  $\beta$ -tocopherol with spike glycoprotein, the RMSD graph of spike glycoprotein-  $\beta$ -tocopherol complex displays the shift in C $\alpha$  atoms position throughout 100-ns MD simulation with RMSD value between 2.172 and 6.884 Å. While the  $\beta$ -tocopherol writes on protein RMSD ranges between 1.254 and 3.321 Å shows good stability with rotational movement of ligand in binding site throughout 100-ns MD simulation (Fig. 2A). The RMSD value of spike-RBD-ACE2 protein-  $\beta$  sitosterol complex protein C $\alpha$  was ranged between 1.199 and 3.585 Å indicating less positional movement, while ligand writes on protein RMSD value 1.117 and 18.14 Å shows the great movement of ligand on protein in respect to their initial position on protein (Fig. 2D). Based on the atom selection, the RMSD was determined after all protein frames were aligned on the reference frame backbone. As observed in Fig. 2D, the C $\alpha$  protein atoms fluctuated in the range of 2.172–6.884 Å and finally stabilized after 40 ns of simulation with an RMSD value of 6.0 Å. The higher fluctuation (6.8 Å) in RMSD of protein

**Table 3** Docking interactions of identified MOL phytoconstituents with SARS-CoV-2 spike receptor-binding domain bound with ACE2 (spike RBD-ACE2; PDB ID: 6M0J) using AutoDock 4.2 and AutoDockVina. AccelrysBiovia Discovery Studio version 2017 R2 was used to visualize interacting amino acid residues. In AutoDock 4.2, the ligand–protein interaction is represented by Ball and Stick model, while in AutoDockVina, it is represented by a 2-D line model. Dark green-dotted line represents the H-bond, whereas the alkyl and pi-alkyl bond interactions are represented by magenta broken lines

S. No.	Ligands with MF and MW and PubChem CID	AutoDockV4.2		Interacting amino acids	Autodock Vina	
		BE (Kcal/mol)	K <sub>d</sub>		BE (kcal/mol)	Interacting amino acids
1.	4-morpholinepropanamine; N-(3-Aminopropyl)morpholine PubChem CID: 61055 MF: C7H16N2O MW: 144.21	-6.36	21.8 4 μM		-4.1	
2.	Piperidine, (phenylmethyl)- [2-Benzylpiperidine] PubChem CID: 118004 MF: C12H17N MW: 175	-6.96	7.98 μM		-6.7	
3.	Guanosine PubChemCID:13539 8635 MF: C10H13NSO5 MW: 283	-7.3	4.49 μM		-7.5	
4.	Hexatriacontane PubChem CID: 12412 MF: C36H74 MW: 506	-6.24	26.5 1 μM		-7.7	

Active site: Glu402

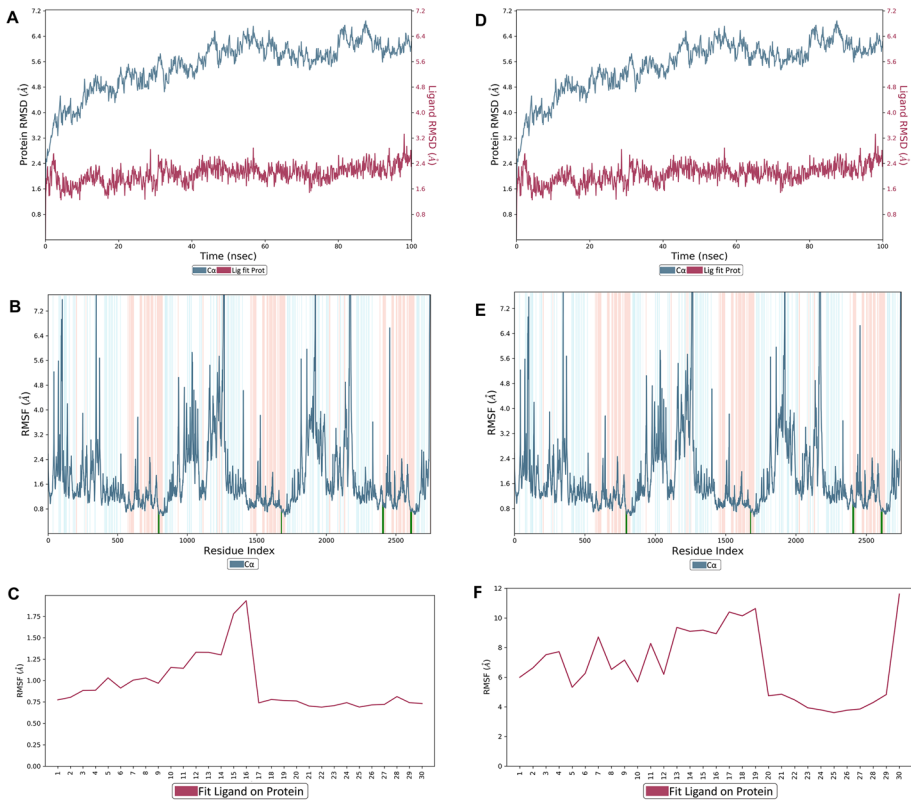
**Table 3** (continued)

5.	2,8-dimethyl-2-(4,8,12-trimethyltridecyl)-6-chromanol	-6.16	30.4 8 $\mu$ M	-7.9
	PubChem			
	CID: 586837			
	MF: C <sub>27</sub> H <sub>46</sub> O <sub>2</sub>			
	MW: 402			
				
	Active site: Glu375,His345,Pro346			
6.	beta.-Tocopherol	-6.02	38.5 5 $\mu$ M	-7.6
	PubChem			
	CID: 6857447			
	MF: C <sub>28</sub> H <sub>48</sub> O <sub>2</sub>			
	MW: 416			
				
	Active site: Glu375,Pro346, Glu402			
7.	gamma.-Tocopherol	-6.93	8.28 $\mu$ M	-8.2
	PubChem			
	CID: 92729			
	MF: C <sub>28</sub> H <sub>48</sub> O <sub>2</sub>			
	MW: 416			
				
	Active site: Glu375,Pro346, Glu402			
8.	Ergost-5-en-3-ol, (3.beta.)-	-8.06	1.24 $\mu$ M	-9.2
	Campesterol			
	PubChem			
	CID: 173183			
	MF: C <sub>28</sub> H <sub>48</sub> O			
	MW: 400			
				
	Active site:Glu402, His378			
				

$C\alpha$  was observed at 82 and 88 ns, while in the case of ligand, the very little fluctuation was observed throughout simulation time. Throughout the simulation, a stable hydrophobic interaction was observed with Gln1002. Alternatively,  $\beta$ -sitosterol with spike RBD-ACE2 protein, RMSDs of protein ( $C\alpha$ ), and ligand was observed in the range of 1.1–3.5 Å and 1.1–18.1 Å, respectively (Fig. 2D). Throughout the simulation, ligand–protein interaction and stable configuration were observed in the range of 50–80-ns simulation.

**Table 3** (continued)

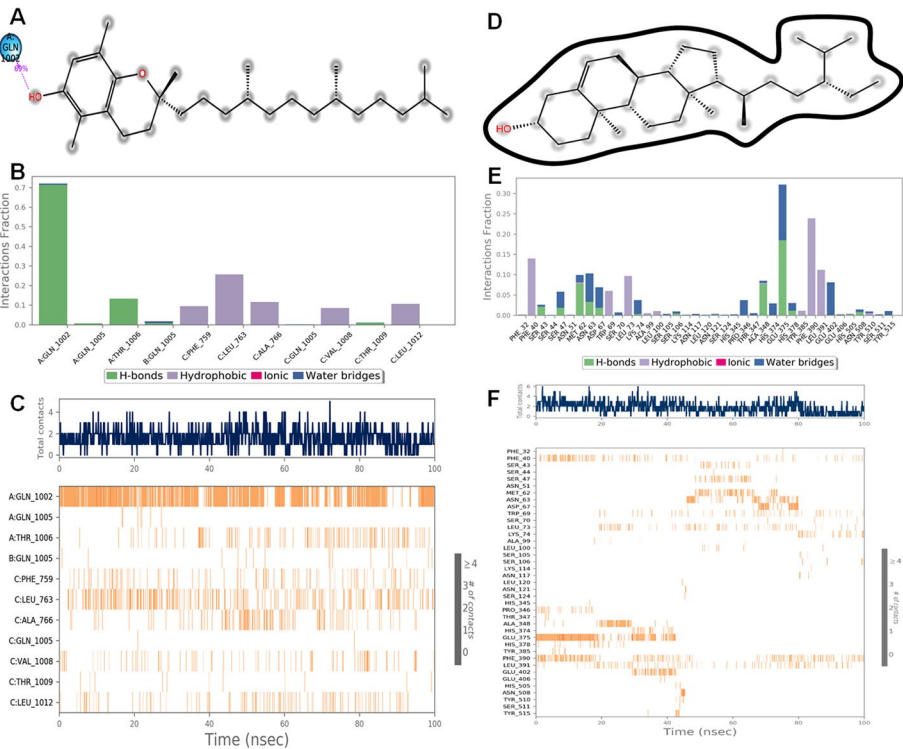
<p>9. dl-<math>\alpha</math>-Tocopherol PubChem CID: 2116 MF: C<sub>29</sub>H<sub>50</sub>O<sub>2</sub> MW: 430</p>	<p>-6.3 24.0 6 <math>\mu</math>M</p>		<p>-8.0</p>			
<p>10. Stigmasta-5,22-dien-3-ol, (3<math>\beta</math>,22<math>\epsilon</math>)- PubChem CID: 6432745 MF: C<sub>29</sub>H<sub>48</sub>O MW: 412</p>	<p>-8.25 903.03 nM</p>		<p>-9.2</p>			
<p>Activesite: Glu375, Glu402, His378</p>		<p>11. Stigmast-5-en-3-ol, (3<math>\beta</math>,20<math>\beta</math>)- <b>betaSitoosterol</b> PubChem CID: 222284 MF: C<sub>29</sub>H<sub>50</sub>O MW: 414</p>	<p>-8.66 452.53 <math>\mu</math>M</p>		<p>-9.6</p>	
<p>Active site: Glu375, His345, Pro346, Glu402, His378</p>		<p>12. Fucosterol PubChem CID: 5281328 MF: C<sub>29</sub>H<sub>48</sub>O MW: 412</p>	<p>-8.11 1.14 <math>\mu</math>M</p>		<p>-9.5</p>	
<p>13. Lupeol PubChem CID: 259846 MF: C<sub>30</sub>H<sub>50</sub>O MW: 426</p>	<p>-7.96 1.46 <math>\mu</math>M</p>		<p>-8.2</p>			
<p>Active site: Glu375, His345, Pro346, Glu402, His378</p>		<p>Active site: His378</p>				



**Fig. 2** Molecular dynamics simulation of ligands in complex with proteins of SARS-CoV-2 during 100-ns time scale. **A** and **D** RMSD value of  $\beta$ -tocopherol in complex with spike glycoprotein (PDB ID: 6VYB) and  $\beta$ -sitosterol in complex with spike receptor-binding domain bound with ACE2 (spike RBD-ACE2; PDB ID: 6M0J), respectively, which was obtained from three independent 100-ns runs. **B** and **E** RMSF value of  $\beta$ -tocopherol in complex with spike glycoprotein (PDB ID: 6VYB) and  $\beta$ -sitosterol in complex with spike receptor-binding domain bound with ACE2 (spike RBD-ACE2; PDB ID: 6M0J), respectively, at 100-ns simulation run from three independent runs. The curve in light blue curves shows protein residue fluctuations, and green-colored vertical bars display the protein residues interacting with ligand. The  $\alpha$ -helical and  $\beta$ -strand regions are highlighted in red and blue backgrounds, respectively. **C** and **F** Showing characterizing changes in the ligand atom positions of  $\beta$ -tocopherol and  $\beta$ -sitosterol RMSF, respectively

The flexibility of amino acid residues on ligand binding was analyzed using RMSFs metrics (Fig. 2B). During protein–ligand simulation, RMSF graph’s peaks showed the fluctuation of C $\alpha$  atoms of the protein. For this, RMSF analysis of SARS-CoV-2 spike glycoprotein and spike RBD-ACE2 protein was executed to understand the conformational changes in the structure. The  $\beta$ -tocopherol was identified to interact with SARS-CoV-2 spike glycoprotein amino acids residing in the vicinity of  $\alpha$ -helices (green lines) and displaying good stability, because  $\alpha$  helices are less prone to oscillations due to intrachain hydrogen bonding. The RMSF graph of spike glycoprotein-  $\beta$ -tocopherol protein C $\alpha$  atoms display changes in protein secondary structure throughout 100-ns MD simulation with RMSF value of protein C $\alpha$  atom ranging between 0.45 and 9.93 Å (Fig. 2B), while C $\alpha$  atom amino acid interacting with  $\beta$ -tocopherol was found between 0.62 and 0.94 (Fig. 2C). These interacting residues allowed tocopherol to search for a good minimum energy position to associate with the surrounding residues in the SARS-Co-2 spike

glycoprotein binding site. Alternatively,  $\beta$ -sitosterol was found to interact with SARS-CoV-2 spike RBD-ACE2 protein amino acid residues lying primarily in the province of  $\alpha$ -helices (green lines), except at 325 amino acid residue index showing  $\beta$ -strand (blue lines); thus, this complex also displayed good stability. The RMSF graph of spike-RBD-ACE2-  $\beta$ -sitosterol was indicating good stability of protein secondary structure with RMSF value of 0.57–4.46 Å (Fig. 2F) and C $\alpha$  atom of amino acid interacting with  $\beta$ -sitosterol ranged between 0.63–1.77 Å (Fig. 2E). Thus, in terms of binding energy and  $K_d$  values, this data indicated that  $\beta$ -sitosterol displayed a good binding affinity with protein. Interestingly, due to reduced fluctuation of C $\alpha$  atoms of SARS-CoV-2 spike RBD-ACE2 protein, the RMSD value of  $\beta$ -sitosterol displayed less variation, and created a more stable complex than SARS-CoV-2 spike glycoprotein-  $\beta$ -sitosterol complex (Fig. 2A and D).



**Fig. 3** Interaction diagram of ligands with SARS-CoV-2 protein during 100-ns simulation. **A** and **D** A schematic of detailed  $\beta$ -tocopherol atom interactions with spike glycoprotein (PDB ID: 6VYB) amino acid residues and  $\beta$ -sitosterol with spike receptor-binding domain bound with ACE2 (spike RBD-ACE2; PDB ID: 6MOJ) amino acid residues, respectively. The selected trajectory displays interactions that take up more than 30% of the simulation run time. **B** and **E** The interaction fraction of  $\beta$ -tocopherol with spike glycoprotein and  $\beta$ -sitosterol with spike RBD-ACE2 was determined during 100-ns simulation. As seen in the plot above, these interactions can be classified depending upon interaction type. Hydrophobic, hydrogen bond, ionic, and water bridges are the four forms of protein–ligand interactions (or “contacts”). **C** and **F** A time-line illustrations of the interactions and contacts of  $\beta$ -tocopherol with spike glycoprotein and  $\beta$ -sitosterol with spike RBD-ACE2, respectively. The total number of specific contacts the protein makes with the ligand during the course of the trajectory is shown in the top panel. In each trajectory frame, the bottom panel displays the residues interacting with the ligand. As per the scale to the right of the plot, the residues making many contact are displayed by a darker shade of orange



Fig. 3A and D show the 2D-trajectory diagram of ligand atom and protein residues interactions, viz.  $\beta$ -tocopherol to SARS-Co-2 spike glycoprotein and  $\beta$ -sitosterol to SARS-CoV-2 spike RBD-ACE2 protein residues, respectively. Interactions that lasted for more than 30% of the simulation time were considered. Protein–ligand contact analysis displayed the presence of H-bond, hydrophobic, and water bridges interactions. Further, the protein–ligand contact analysis of the MD simulation result was assessed against both spike glycoprotein and spike RBD-ACE2 protein. Both proteins were found to share multiple types of interaction such H-bond, hydrophobic bond, ionic interaction, and water bridges with their respective ligands. Fig. 3B depicts that the hydrogen bond formed with  $\beta$ -tocopherol ligand in the docking pose which maintained 70% of the simulation time, which is followed by hydrophobic and water bridges interactions. A total of 11 amino acid residues contacts were formed with ligand from Gln1002 to Leu1012 (Fig. 3C). The histogram of spike glycoprotein-  $\beta$ -tocopherol displayed that Gln 1002 from A-chain made most significant interaction with  $\beta$ -tocopherol involving H-bond and water bridges which provide the stability of complex throughout the 100-ns MD simulation. While Gln1005 and Thr 1006 from A-chain, and Gln 1005 from B-chain were also found to be interacting with  $\beta$ -tocopherol with H-bond and water bridges, the C-chain amino acids Phe 759, Leu 763, Ala 766 Gln1005, Val1008, and Leu1012 play a major role in hydrophobic interactions. Thr 1009 from C-chain display minor H-bond interaction with  $\beta$ -tocopherol (Fig. 3B and C). Interestingly, these existing interactions in MD throughout the trajectory were also revealed by molecular docking analyses (Table 2). Fig. 3E depicts that the water bridges bond formed with  $\beta$ -sitosterol ligand in the docking pose which maintained 30% of the simulation time, which is followed by hydrophobic and H-bond interactions. A total of 39 amino acid residues contacts were formed with ligand from Phe32 to Tyr515 (Fig. 3F). A profound analysis of spike RBD-ACE2 - $\beta$ -sitosterol contact analysis revealed that Glu 375 was major H-bond contributing amino acid, and it also formed major water bridge, while Phe 32, Trp69, Leu73, Phe390, and Leu 391 were major water bridge interaction contributor. Beside Glu 375, other amino acid also contributes in water bridge interaction between beta-sitosterol. A detailed interaction of spike glycoprotein-  $\beta$ -tocopherol complex and spike-RBD-ACE2 protein-  $\beta$  sitosterol in protein–ligand contact analysis were represented in Table 4. The result of all amino acid residues in molecular docking interaction of ligand molecule with the target protein was also revealed during the dynamic simulation analysis, which indicated the stable configuration and minimal backbone fluctuations of ligand–protein complex. During the MD analysis, the simulation showed more water-mediated interactions with hit molecules. A similar kind of ligand–protein complex stability and interactions was also studied by a previous study which supports our results [37]. Less variation in the complex structure is an indication of greater stability [36]. Surprisingly, both complexes, especially the  $\beta$ -sitosterol-spike RBD-ACE2 protein, showed low deviations over 100-ns timescales, indicating good protein–ligand stability and compactness (Fig. 2A and D). Some recently published studies have analyzed in silico computational analysis using randomly selected compounds from the plant origin [38, 39]; however, in this study, GC–MS analysis of MOL extract was performed to find out the active phytoconstituents and then analyzed their binding effects. A previous study has reported the protein–ligand complexes stability with SARS-CoV-2 Mpro using three main flavonoids isorhamnetin, kaempferol, and apigenin at 100-ns simulation, which demonstrated a strong binding affinity and a stable configuration throughout the simulation [38]. Likewise, another study has reported the simulation analysis of ellagic acid and apigenin phytoconstituents from *Moringa oleifera* against nsp9/10 of SARS-CoV-2 at 30-ns timescale, in which ellagic acid was found to be more noticeable on nsp9 as compared to apigenin for nsp10 [39].

**Table 4** A detailed interaction of amino acid residues of spike glycoprotein-  $\beta$ -tocopherol complex and spike-RBD-ACE2 protein-  $\beta$  sitosterol in protein–ligand contact analysis

Protein–ligand contact analysis			
S. no	Interaction	Spike glycoprotein- $\beta$ -tocopherol complex	Spike-RBD-ACE2 protein- $\beta$ sitosterol
1	H-bonds	A: Gln 1002, Gln 1005, Thr1006 B: Gln 1005 C: Thr1009	Ser 43, Ser44, Ser 47, Met62, Asn63, Asp 67, Lys74, Ser106, Asn121, Ala348, Glu375, His378, His505, Asn508
2	Hydrophobic	C: Phe 759, Leu763, Ala766, Gln1005, Val1008, Leu1012	Phe 32, Phe40, Met62, Trp69, Leu73, Ala99, Leu100, Ala348, Tyr385, Phe390, Leu391, Tyr510
3	Ionic		
4	Water bridges	B: Gln 1005	Ser43, Ser47, Asn 51, Met62, Asn63, Asp 67, Ser70, Lys 74, Ser105, Ser106, Lys 114, Asn117, Leu120, Asn121, Ser124, His345, Pro346, Thr347, Ala348, His374, Glu375, His378, Glu402, Glu406, His505, Asn508, Tyr510, Ser511, Tyr515

The  $\beta$ -tocopherol is a type of tocopherol bearing a long side chain in heterocyclic nucleus [40]. It possesses vitamin E activity and hence fat-soluble antioxidants and thus easily penetrates biological membranes. Various *in vitro*, *in vivo*, and clinical studies have also revealed the potential antiviral activity of  $\beta$ -tocopherol, for instance, in the modulation of host micro-RNA in patients with hepatitis B virus-related persistent infection [41], antiviral effect against influenza virus-infected mice [42], and enhancement of cell-mediated and humoral immune responses [43]. On the other hand,  $\beta$ -sitosterol is a member of class phytosterols with chemical structures similar to that of cholesterol which possesses antioxidant and anti-inflammatory activity [44]. Many previous studies have shown the potential antiviral activity of  $\beta$ -tocopherol, for instance, protection of mice from pre-administered  $\beta$ -sitosterol from lethal influenza A virus infection, anti-hepatitis B virus activity tested in hepatoblastoma line and *in silico* confirmation with hepatitis B virus Pol active-site residues [45], and viral plaque inhibitory effect against African swine fever virus and Herpes simplex virus [46].

### PASS Analysis, Lipinski's Rule of 5, and Toxicity Assessment

Further, to find the physicochemical and toxicity profile of the best hits for drug-likeness, sixteen phytomolecules were investigated using an offline Data Warrior 5.2.1 and online Molinspiration chemoinformatic tool. Table 5 shows the physicochemical properties of MOL phytoconstituents using Lipinski's rule of 5. Lipinski's violation should be comparable to that of an orally active medication [47]. Except for hexatriacontane (Lipinski's violation=two), nearly all MOL phytoconstituents had only one violation of Lipinski's rule of five. The drug-likeness and toxicity potential of MOL bioactive components are shown in Table 6. Except for fucosterol and E,E,Z-1,3,12-Nonadecatriene-5,14-diol, the results showed that all components are safe to use and have no known toxicity in terms of reproductive unfavorable effects, mutagenic, tumorigenic, or irritant.

### Physicochemical and Pharmacokinetic (ADMET) Properties of Phytocomponents

To see whether particular phytoconstituents of MOL might be used in pharmacokinetic studies, the online SwissADME program was used to compute ADMET characteristics (Table 7). All components except guanosine were determined to be lipid soluble based on the computed LogP value, indicating good absorption across the skin. P-gp is a protein pump that removes substances from biological systems. It is ATP-dependent. P-gp is extremely expressed in cancer and virally infected cells [48]. Table 7 shows that all components (except two) do not have blood–brain barrier (BBB) permeability, and half of them do not have permeability-gp (P-gp) substrates. Because the virus is also an intracellular pathogen, only half of the identified components of MOL are likely to stay in the cells and have bioavailability, as well as could exhibit their intracellular pharmacological activity. Cytochromes P450 (CYPs) are a group of key metabolic enzymes that play a role in xenobiotic biotransformation. Xenobiotic can function as both substrate and inhibitor of cytochromes P450, which are involved in the metabolism of the majority of pharmaceuticals. Inhibitors of the five classes of CYPs induce an elevation in their plasma concentrations, resulting in enhanced bioavailability. Surprisingly, none of the MOL components (except for a few) were shown to be inhibitors of any of the five CYP classes (Table 7). The skin permeability (K<sub>p</sub>) is a unit of measurement that quantifies the rate of chemical penetration through the skin's epidermis. Except for hexacosane and hexatriacontane, all phytocomponents had a negative K<sub>p</sub> value, indicating that topical absorption of these phytoconstituents is unlikely. Table 7 shows that the components

**Table 5** PASS analysis of identified bioactive chemicals from MOL extract

S. no	Phytoconstituents	% Absorption <sup>a</sup> (>50%)	Topological polar surface area (TPSA) (Å) <sup>2</sup> , <sup>b</sup> (<160 Å)	MW (≤500)	c logP <sup>c</sup> (≤5)	Heavy atom count (n atoms)	Hydrogen bond donors (nOHNH) (≤5)	Hydrogen bond acceptors (nON) (≤10)	Number of rotatable bonds (≤10)	Lipinski's violation
1	N-(3-Aminopropyl)morpholine	95.72	38.49	144.2	-0.75	10	2	3	3	0
2	2-Benzylpiperidine	104.84	12.03	175.28	2.80	13	1	1	2	0
3	Guanosine	53.96	159.52	283.24	2.02	20	6	10	2	1
4	Hexatriacontane	0.0	0.0	506.99	10.47	36	0	0	33	2
5	2,8-dimethyl-2-(4,8,12-trimethyltridecyl)-6-chromanol	79.00	86.95	322.41	-0.74	23	2	7	3	0
6	beta-Tocopherol	98.83	29.46	416.69	8.98	30	1	2	12	1
7	gamma-Tocopherol	98.83	29.46	416.69	8.98	30	1	2	12	1
8	Campesterol	102.02	20.23	400.69	8.30	29	1	1	5	1
9	dl-alpha-Tocopherol	98.83	29.46	430.72	9.04	31	1	2	12	1
10	Stigmasta-5,22-dien-3-ol, (3.beta.,22e)-	102.02	20.23	412.70	7.87	30	1	1	5	1
11	BetaSitosterol	102.02	20.23	414.72	8.62	30	1	1	6	1
12	Fucosterol	102.02	20.23	412.70	7.69	30	1	1	5	1
13	Lupeol	102.02	20.23	426.73	8.29	31	1	1	1	0
14	Hexacosane	0.0	0.00	366.72	9.91	26	0	0	23	1
15	Squalene	0.0	0.00	410.73	9.62	30	0	0	15	1
16	E,E,Z-1,3,12-Nonadecatriene-5,14-diol	95.04	40.46	294.48	5.95	21	2	2	14	1

**RULE:**

<sup>a</sup>Percentage absorption was calculated as: % Absorption = 109- [0.345 × TPSA]

<sup>b</sup>Topological polar surface area (defined as a sum of surfaces of polar atoms in a molecule)

<sup>c</sup>Logarithm of compound partition coefficient between n-octanol and water

**Table 6** Drug likeness and toxicity calculation of MOL phytoconstituents

S. no	Compound name	Drug- likeness	Mutant	Tumurogenic	Repro- ductive effective	Irritant
1	N-(3-Aminopropyl)morpholine	0.075381	N	N	N	N
2	2-Benzylpiperidine	-0.7075	N	N	N	N
3	Guanosine	-1.348	N	N	N	N
4	Hexatriacontane	-20.398	N	N	N	N
5	2,8-dimethyl-2-(4,8,12-trimethyltridecyl)-6-chromanol	9.3678	N	N	L	N
6	Beta-Tocopherol	-3.2757	N	N	N	N
7	Gamma-Tocopherol	-3.2757	N	N	N	N
8	Campesterol	-8.1908	N	N	N	N
9	dl-alpha-Tocopherol	-3.2757	N	N	N	N
10	Stigmasta-5,22-dien-3-ol, (3.beta.,22e)-	1.2217	N	N	N	N
11	Beta-Sitosterol	-4.475	N	N	N	N
12	Fucosterol	-6.2842	N	N	N	H
13	Lupeol	-22.172	N	N	N	N
14	Hexacosane	-20.398	N	N	N	N
15	Squalene	-3.5218	N	N	N	N
16	E,E,Z-1,3,12-Nonadecatriene-5,14-diol	-20.672	N	N	N	H

*N* no toxicity

*L* low toxicity

*H* high toxicity

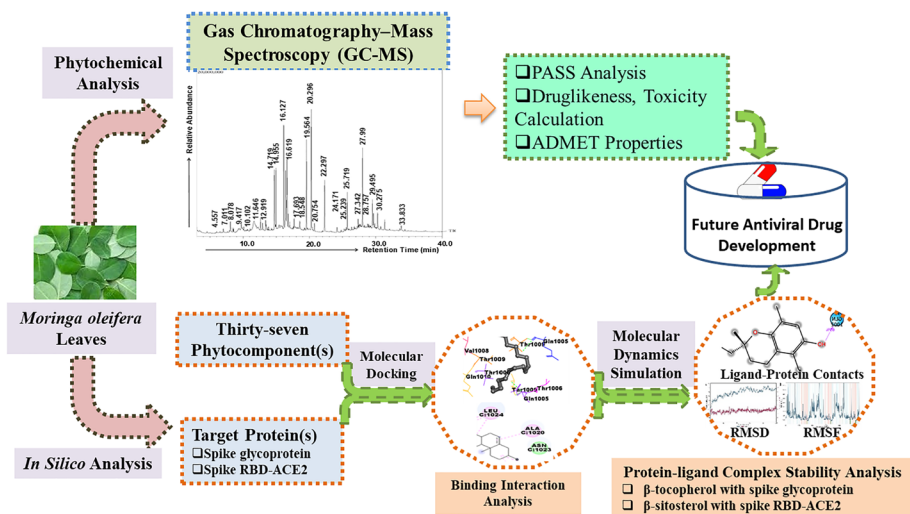
N-(3-Aminopropyl) morpholine, 2-Benzylpiperidine, and E,E,Z-1,3,12-Nonadecatriene-5,14-diol are probably to be digested further and are susceptible to being absorbed from the GI tract quickly, hence enhancing plasma levels and bioavailability. Both phytochemical analysis of *Moringa oleifera* phytoconstituents and in silico analysis of antiviral drug development are represented pictorially in Fig. 4.

## Conclusion

Phytochemical investigation of MOL extract through GC–MS showed thirty-seven active components of terpenes, polyphenols, fatty acids, phytosterols, and aliphatic hydrocarbons classes. The top sixteen hits showed a strong binding affinity with SARS-CoV-2 spike glycoprotein and spike RBD-ACE2 protein. During 100-ns simulation, the best hits,  $\beta$ -tocopherol with spike glycoprotein and  $\beta$ -sitosterol with spike RBD-ACE2, showed low deviations, indicating good stability and compactness of both ligand–protein complexes. Most of the phytoconstituents of MOL displayed drug- likeness with no predicted toxicity. Interestingly, the best hits  $\beta$ -tocopherol and  $\beta$ -sitosterol have also shown drug- likeness and no toxicity profile. Based on these findings, all these components particularly  $\beta$ -sitosterol and  $\beta$ -tocopherol can be formulated as targeted therapeutic agents against SARS-CoV-2 spike glycoprotein and spike RBD-ACE2 protein.

**Table 7** Calculation of ADMET properties of MOL phytochemicals using online SwissADME software

S. no	Phytochemicals	Lipophilicity (consensus Log Po/w)	BBB permeant	P-gp substrate	CYP1A2 inhibitor	CYP2C19 inhibitor	CYP2C9 inhibitor	CYP2D6 inhibitor	CYP3A4 inhibitor	Log Kp (skin permeation)	GI absorption
1	N-(3-Aminopropyl)morpholine	0.15	No	No	No	No	No	No	No	- 7.67	High
2	2-Benzylpiperidine	2.60	Yes	No	No	No	Yes	No	No	- 5.48	High
3	Guanosine	-2.02	No	No	No	No	No	No	No	-9.37	Low
4	Hexatriacontane	13.67	No	Yes	No	No	No	No	No	4.18	Low
5	2,8-dimethyl-2-(4,8,12-trimethyltridecyl)-6-chromanol	7.58	No	Yes	No	No	No	No	No	- 1.68	Low
6	Beta-Tocopherol	7.79	No	Yes	No	No	No	No	No	- 1.51	Low
7	Gamma-Tocopherol	7.95	No	Yes	No	No	No	No	No	- 1.51	Low
8	Campesterol	6.90	No	No	No	No	No	No	No	- 2.50	Low
9	dl-alpha-Tocopherol	8.27	No	Yes	No	No	No	No	No	- 1.33	Low
10	Stigmasta-5,22-dien-3-ol, (3.beta.,22e)-	6.97	No	Yes	No	Yes	No	No	No	- 2.74	Low
11	Beta-Sitosterol	7.19	No	No	No	No	No	No	No	- 2.20	Low
12	Fucosterol	7.07	No	No	No	No	No	No	No	- 2.53	Low
13	Lupeol	7.26	No	No	No	No	No	No	No	- 1.90	Low
14	Hexacosane	10.09	No	Yes	No	No	No	No	No	1.19	Low
15	Squalene	9.38	No	No	No	No	No	No	No	- 0.58	Low
16	E,E,Z-1,3,12-Nonadecatriene-5,14-diol	4.94	Yes	Yes	Yes	Yes	Yes	Yes	Yes	- 4.08	High



**Fig. 4** Pictorial representation of the phytochemical analysis and in silico antiviral drug development evaluation of *Moringa oleifera* phytoconstituents

## Limitations of the Study

In current study, the binding interaction of best hits  $\beta$ -tocopherol and  $\beta$ -sitosterol with SARS-CoV-2 spike glycoprotein and spike RBD-ACE2 protein, respectively, is a predictive nature of the study based on computational approach. In addition, the use of only 100-ns MD simulations of the protein–ligand complex, which is insufficient to warrant the subsequent detailed analysis of interactions. Further, the SARS-CoV-2 spike glycoprotein contains certain missing residues that should be added, and/or a modeled protein is required for further investigation. To compare the structural changes, a protein simulation (without ligand) is also required.

**Supplementary Information** The online version contains supplementary material available at <https://doi.org/10.1007/s12010-022-04040-1>.

**Acknowledgements** The authors extend their appreciation to the Deanship of Scientific Research at the King Khalid University for financial support through the Small Groups Project under grant number (RGP. 1/218/43). The authors are also acknowledged for tissue culture facilities to the Department of Biotechnology, Era University, Lucknow, India.

**Author Contribution** Sahabjada Siddiqui, Shivbrat Upadhyay, and Rumana Ahmad conceived and directed the study; Sahabjada Siddiqui, Shivbrat Upadhyay, and Tanveer Ahamad carried out the experimental work; Sahabjada Siddiqui, Shivbrat Upadhyay, Md. Abul Barkat, Azfar Jamal, Abdulaziz S. Alothaim, Mohd. Zaheen Hassan, Mohammad Akhlaquer Rahman, Md Arshad, Tanveer Ahamad, Mohammad Faheem Khan, Hari Shankar, M Ali, Sarjeel Kaleem, and Jalal Ahmad analyzed and interpreted the results. Md. Abul Barkat, Mohd. Zaheen Hassan, Mohammad Akhlaquer Rahman, Md Arshad, Hari Shankar, M Ali, and Sarjeel Kaleem provide critical inputs and revised the manuscript. All authors contributed to the manuscript writing, editing, and final proof.

**Data Availability** All data were obtained from the experiments, and third party is not involved in any data or materials in this manuscript.

## Declarations

**Ethical Approval** Not applicable.

**Consent to Participate** All authors agree to participate in and publish this work, and they affirm that it is original research.

**Consent to Publish** If the manuscript is accepted, the term and condition of the publisher will be followed.

**Competing Interests** The authors declare no competing interests.

## References

1. Altakarli, N. S. (2020). China's response to the COVID-19 outbreak: A model for epidemic preparedness and management. *Dubai Medical Journal*, 3(2), 44–49. <https://doi.org/10.1159/000508448>
2. Atolani, O., Baker, M. T., Adeyemi, O. S., Olanrewaju, I. R., Hamid, A. A., Ameen, O. M., & Usman, L. A. (2020). COVID-19: Critical discussion on the applications and implications of chemicals in sanitizers and disinfectants. *EXCLI journal*, 19, 785. <https://doi.org/10.17179/excli2020-1386>
3. Payne, S. (2017). Family Coronaviridae. *Viruses*, 149. <https://doi.org/10.1016/B978-0-12-803109-4.00017-9>
4. Pal, M., Berhanu, G., Desalegn, C., & Kandi, V. (2020). Severe acute respiratory syndrome coronavirus-2 (SARS-CoV-2): An update. *Cureus*, 12(3). <https://doi.org/10.7759/cureus.7423>
5. Du, L., He, Y., Zhou, Y., Liu, S., Zheng, B. J., & Jiang, S. (2009). The spike protein of SARS-CoV—a target for vaccine and therapeutic development. *Nature Reviews Microbiology*, 7(3), 226–236. <https://doi.org/10.1038/nrmicro2090>
6. Shang, J., Wan, Y., Luo, C., Ye, G., Geng, Q., Auerbach, A., & Li, F. (2020). Cell entry mechanisms of SARS-CoV-2. *Proceedings of the National Academy of Sciences*, 117(21), 11727–11734. <https://doi.org/10.1073/pnas.2003138117>
7. Pandey, M. M., Rastogi, S., & Rawat, A. K. S. (2013). Indian traditional ayurvedic system of medicine and nutritional supplementation. *Evidence-Based Complementary and Alternative Medicine*, 2013. <https://doi.org/10.1155/2013/376327>
8. Shah, B. N. (2009). *Textbook of pharmacognosy and phytochemistry*. Elsevier India.
9. Pandey, A., Pradheep, K., Gupta, R., Nayar, E. R., & Bhandari, D. C. (2011). 'Drumstick tree' (*Moringa oleifera* Lam.): A multipurpose potential species in India. *Genetic Resources and Crop Evolution*, 58(3), 453–460. <https://doi.org/10.1007/s10722-010-9629-6>
10. Anwar, F., Latif, S., Ashraf, M., & Gilani, A. H. (2007). *Moringa oleifera*: A food plant with multiple medicinal uses. *Phytotherapy Research: An International Journal Devoted to Pharmacological and Toxicological Evaluation of Natural Product Derivatives*, 21(1), 17–25. <https://doi.org/10.1002/ptr.2023>
11. Abdull Razis, A. F., Ibrahim, M. D., & Kntayya, S. B. (2014). Health benefits of *Moringa oleifera*. *Asian pacific journal of cancer prevention*, 15(20), 8571–8576. <https://doi.org/10.7314/apjcp.2014.15.20.8571>
12. Meireles, D., Gomes, J., Lopes, L., Hinzmann, M., & Machado, J. (2020). A review of properties, nutritional and pharmaceutical applications of *Moringa oleifera*: Integrative approach on conventional and traditional Asian medicine. *Advances in Traditional Medicine*, 20(4), 495–515. <https://doi.org/10.1007/s13596-020-00468-0>
13. Vergara-Jimenez, M., Almatrafi, M. M., & Fernandez, M. L. (2017). Bioactive components in *Moringa oleifera* leaves protect against chronic disease. *Antioxidants*, 6(4), 91. <https://doi.org/10.3390/antiox6040091>
14. Siddiqui, S., Ahmad, E., Gupta, M., Rawat, V., Shivnath, N., Banerjee, M., & Arshad, M. (2015). *Cissus quadrangularis* Linn exerts dose-dependent biphasic effects: Osteogenic and anti-proliferative, through modulating ROS, cell cycle and Runx2 gene expression in primary rat osteoblasts. *Cell proliferation*, 48(4), 443–454. <https://doi.org/10.1111/cpr.12195>
15. <https://pubchem.ncbi.nlm.nih.gov/> (accessed on May, 2022)
16. Siddiqui, S., Upadhyay, S., Ahmad, R., Gupta, A., Srivastava, A., Trivedi, A., & Khan, M. A. (2020). Virtual screening of phytoconstituents from miracle herb *nigella sativa* targeting




- nucleocapsid protein and papain-like protease of SARS-CoV-2 for COVID-19 treatment. *Journal of Biomolecular Structure and Dynamics*, 1–21. <https://doi.org/10.1080/07391102.2020.1852117>.
17. Oprea, T. I., Davis, A. M., Teague, S. J., & Leeson, P. D. (2001). Is there a difference between leads and drugs? A historical perspective. *Journal of chemical information and computer sciences*, 41(5), 1308–1315. <https://doi.org/10.1021/ci010366a>
  18. Khan, T., Lawrence, A. J., Azad, I., Raza, S., Joshi, S., & Khan, A. R. (2019). Computational drug designing and prediction of important parameters using in silico methods-A review. *Current Computer-Aided Drug Design*, 15(5), 384–397. <https://doi.org/10.2174/1573399815666190326120006>
  19. Daina, A., Michielin, O., & Zoete, V. (2017). SwissADME: A free web tool to evaluate pharmacokinetics, drug-likeness and medicinal chemistry friendliness of small molecules. *Scientific reports*, 7(1), 1–13. <https://doi.org/10.1038/srep42717>
  20. Popova, M., Dimitrova, R., Al-Lawati, H. T., Tsvetkova, I., Najdenski, H., & Bankova, V. (2013). Omani propolis: Chemical profiling, antibacterial activity and new propolis plant sources. *Chemistry Central Journal*, 7(1), 1–8. <https://doi.org/10.1186/1752-153X-7-158>
  21. Pitt, J. J. (2009). Principles and applications of liquid chromatography-mass spectrometry in clinical biochemistry. *The Clinical Biochemist Reviews*, 30(1), 19.
  22. Rakib, A., Paul, A., Chy, M., Uddin, N., Sami, S. A., Baral, S. K., & Simal-Gandara, J. (2020). Biochemical and computational approach of selected phytochemicals from *inospora crista* in the management of COVID-19. *Molecules*, 25(17), 3936. <https://doi.org/10.3390/molecules25173936>
  23. Alam, R., Imon, R. R., Talukder, M. E. K., Akhter, S., Hossain, M. A., Ahammad, F., & Rahman, M. M. (2021). GC-MS analysis of phytoconstituents from *Ruellia prostrata* and *Senna tora* and identification of potential anti-viral activity against SARS-CoV-2. *Rsc Advances*, 11(63), 40120–40135. <https://doi.org/10.1039/D1RA06842C>
  24. Wen, C. C., Kuo, Y. H., Jan, J. T., Liang, P. H., Wang, S. Y., Liu, H. G., & Yang, N. S. (2007). Specific plant terpenoids and lignoids possess potent antiviral activities against severe acute respiratory syndrome coronavirus. *Journal of medicinal chemistry*, 50(17), 4087–4095. <https://doi.org/10.1021/jm070295s>
  25. Bhuiyan, F. R., Howlader, S., Raihan, T., & Hasan, M. (2020). Plants metabolites: Possibility of natural therapeutics against the COVID-19 pandemic. *Frontiers in Medicine*, 444. <https://doi.org/10.3389/fmed.2020.00444>
  26. Guy, J. L., Jackson, R. M., Jensen, H. A., Hooper, N. M., & Turner, A. J. (2005). Identification of critical active-site residues in angiotensin-converting enzyme-2 (ACE2) by site-directed mutagenesis. *The FEBS journal*, 272(14), 3512–3520. <https://doi.org/10.1111/j.1742-4658.2005.04756.x>
  27. Teli, D. M., Shah, M. B., & Chhabria, M. T. (2021). In silico screening of natural compounds as potential inhibitors of SARS-CoV-2 main protease and spike RBD: Targets for COVID-19. *Frontiers in molecular biosciences*, 7, 429. <https://doi.org/10.3389/fmolb.2020.599079>
  28. Singh, R., Bhardwaj, V. K., Sharma, J., Kumar, D., & Purohit, R. (2021). Identification of potential plant bioactive as SARS-CoV-2 Spike protein and human ACE2 fusion inhibitors. *Computers in Biology and Medicine*, 136, 104631. <https://doi.org/10.1016/j.combiomed.2021.104631>
  29. Hiremath, S., Kumar, H. D., Nandan, M., Mantesh, M., Shankarappa, K. S., Venkataravanappa, V., & Reddy, C. N. (2021). In silico docking analysis revealed the potential of phytochemicals present in *Phyllanthus amarus* and *Andrographis paniculata*, used in Ayurveda medicine in inhibiting SARS-CoV-2. *3 Biotech*, 11(2), 1–18. <https://doi.org/10.1007/s13205-020-02578-7>
  30. National Center for Biotechnology Information. PubChem Compound Summary for CID 1742129, (-)-alpha-Tocopherol. <https://pubchem.ncbi.nlm.nih.gov/compound/alpha-Tocopherol>. Accessed Feb. 8, 2022.
  31. Babu, S., & Jayaraman, S. (2020). An update on  $\beta$ -sitosterol: A potential herbal nutraceutical for diabetic management. *Biomedicine and Pharmacotherapy*, 131, 110702. <https://doi.org/10.1016/j.biopha.2020.110702>
  32. Parvez, M. K., Rehman, M. T., Alam, P., Al-Dosari, M. S., Alqasoumi, S. I., & Alajmi, M. F. (2019). Plant-derived antiviral drugs as novel hepatitis B virus inhibitors: Cell culture and molecular docking study. *Saudi Pharmaceutical Journal*, 27(3), 389–400. <https://doi.org/10.1016/j.jsps.2018.12.008>
  33. Zhou, B. X., Li, J., Liang, X. L., Pan, X. P., Hao, Y. B., Xie, P. F., & Zhong, N. S. (2020).  $\beta$ -sitosterol ameliorates influenza A virus-induced proinflammatory response and acute lung injury in mice by disrupting the cross-talk between RIG-I and IFN/STAT signaling. *Acta Pharmacologica Sinica*, 41(9), 1178–1196. <https://doi.org/10.1038/s41401-020-0403-9>
  34. Maurya, V. K., Kumar, S., Bhatt, M. L., & Saxena, S. K. (2022). Antiviral activity of traditional medicinal plants from Ayurveda against SARS-CoV-2 infection. *Journal of Biomolecular Structure and Dynamics*, 40(4), 1719–1735. <https://doi.org/10.1080/07391102.2020.1832577>

35. Kufareva, I., & Abagyan, R. (2011). Methods of protein structure comparison. In *Homology modeling* (pp. 231–257). Humana Press. [https://doi.org/10.1007/978-1-61779-588-6\\_10](https://doi.org/10.1007/978-1-61779-588-6_10)
36. Aier, I., Varadwaj, P. K., & Raj, U. (2016). Structural insights into conformational stability of both wild-type and mutant EZH2 receptor. *Scientific reports*, 6(1), 1–10. <https://doi.org/10.1038/srep34984>
37. KumarFaheem, B. K., Sekhar, K. V. G. C., Ojha, R., Prajapati, V. K., Pai, A., & Murugesan, S. (2022). Pharmacophore based virtual screening, molecular docking, molecular dynamics and MM-GBSA approach for identification of prospective SARS-CoV-2 inhibitor from natural product databases. *Journal of Biomolecular Structure and Dynamics*, 40(3), 1363–1386. <https://doi.org/10.1080/07391102.2020.1824814>
38. Sen, D., Bhaumik, S., Debnath, P., & Debnath, S. (2021). Potentiality of Moringaoleifera against SARS-CoV-2: Identified by a rational computer aided drug design method. *Journal of Biomolecular Structure and Dynamics*, 1–18. <https://doi.org/10.1080/07391102.2021.1898475>
39. Muhammad, S., Hassan, S. H., Al-Sehemi, A. G., Shakir, H. A., Khan, M., Irfan, M., & Iqbal, J. (2021). Exploring the new potential antiviral constituents of Moringa oliefera for SARS-COV-2 pathogenesis: An in silico molecular docking and dynamic studies. *Chemical physics letters*, 767, 138379. <https://doi.org/10.1016/j.cplett.2021.138379>
40. Bergel, F., Jacob, A., Todd, A. R., & Work, T. S. (1938). Vitamin E: Structure of  $\beta$ -tocopherol. *Nature*, 141(3571), 646–646. <https://doi.org/10.1038/141646b0>
41. Fiorino, S., Bacchi-Reggiani, L., Sabbatani, S., Grizzi, F., Di Tommaso, L., Masetti, M., & Pession, A. (2014). Possible role of tocopherols in the modulation of host microRNA with potential antiviral activity in patients with hepatitis B virus-related persistent infection: A systematic review. *British Journal of Nutrition*, 112(11), 1751–1768. <https://doi.org/10.1017/S0007114514002839>
42. Mileva, M., & Galabov, A. S. (2018). Vitamin E and influenza virus infection. *Vitamin E in health and disease*, 67. <https://doi.org/10.5772/intechopen.80954>
43. Lee, G. Y., & Han, S. N. (2018). The role of vitamin E in immunity. *Nutrients*, 10, 1614. <https://doi.org/10.3390/nu10111614>
44. Saeidnia, S., Manayi, A., Gohari, A. R., & Abdollahi, M. (2014). The story of beta-sitosterol-A review. *European journal of medicinal plants*, 4(5), 590. <https://doi.org/10.9734/EJMP/2014/7764>
45. Parvez, M. K., Alam, P., Arbab, A. H., Al-Dosari, M. S., Alhowiriny, T. A., & Alqasoumi, S. I. (2018). Analysis of antioxidative and antiviral biomarkers  $\beta$ -amyrin,  $\beta$ -sitosterol, lupeol, ursolic acid in Guiera senegalensis leaves extract by validated HPTLC methods. *Saudi Pharmaceutical Journal*, 26(5), 685–693. <https://doi.org/10.1016/j.jsps.2018.02.022>
46. Madureira, A. M., Ascenso, J. R., Valdeira, L., Duarte, A., Frade, J. P., Freitas, G., & Ferreira, M. J. U. (2003). Evaluation of the antiviral and antimicrobial activities of triterpenes isolated from Euphorbia segetalis. *Natural Product Research*, 17(5), 375–380. <https://doi.org/10.1080/14786410310001605841>
47. Benet, L. Z., Hosey, C. M., Ursu, O., & Oprea, T. I. (2016). BDDCS, the rule of 5 and drugability. *Advanced drug delivery reviews*, 101, 89–98. <https://doi.org/10.1016/j.addr.2016.05.007>
48. Robinson, K., & Tiriveedhi, V. (2020). Perplexing role of P-glycoprotein in tumor microenvironment. *Frontiers in Oncology*, 10, 265. <https://doi.org/10.3389/fonc.2020.00265>

**Publisher's Note** Springer Nature remains neutral with regard to jurisdictional claims in published maps and institutional affiliations.

## Authors and Affiliations

Sahabjada Siddiqui<sup>1</sup>  · Shivbrat Upadhyay<sup>1</sup> · Rumana Ahmad<sup>2</sup> · Md. Abul Barkat<sup>3</sup> · Azfar Jamal<sup>4,5</sup> · Abdulaziz S. Alothaim<sup>5</sup> · Mohd. Zaheen Hassan<sup>6</sup> · Mohammad Akhlaquer Rahman<sup>7</sup> · Md Arshad<sup>8</sup> · Tanveer Ahamad<sup>1</sup> · Mohammad Faheem Khan<sup>1</sup> · Hari Shankar<sup>9</sup> · M. Ali<sup>10</sup> · Sarjeel Kaleem<sup>11</sup> · Jalal Ahmad<sup>12</sup>

<sup>1</sup> Department of Biotechnology, Era's Lucknow Medical College & Hospital, Era University, Lucknow 226003, India

<sup>2</sup> Department of Biochemistry, Era's Lucknow Medical College and Hospital, Era University, Lucknow, India

<sup>3</sup> Department of Pharmaceutics, College of Pharmacy, University of Hafr Al-Batin, Al Jamiah, Hafr Al Batin 39524, Saudi Arabia

<sup>4</sup> Health and Basic Science Research Centre, Majmaah University, Majmaah 11952, Saudi Arabia

<sup>5</sup> Department of Biology, College of Science, Al-Zulfi, Majmaah University, Majmaah 11952, Riyadh Region, Saudi Arabia

<sup>6</sup> Department of Pharmaceutical Chemistry, College of Pharmacy, King Khalid University, Abha, Saudi Arabia

<sup>7</sup> Department of Pharmaceutics and Industrial Pharmacy, College of Pharmacy, Taif University, Taif 21944, Saudi Arabia

<sup>8</sup> Department of Zoology, Aligarh Muslim University, Aligarh, India

<sup>9</sup> Research Cell, Era's Lucknow Medical College and Hospital, Lucknow, India

<sup>10</sup> Department of Pharmacognosy, College of Pharmacy, Jazan University, Jazan, Saudi Arabia

<sup>11</sup> Avadh Institute of Medical Technologies & Hospital, Lucknow, India

<sup>12</sup> Department of Microbiology, Era's Lucknow Medical College and Hospital, Lucknow, India